# Evaluation of Nonparametric SAR Tomography Methods for Urban Building Reconstruction

Mehrnoosh Omati, Mahmod Reza Sahebi, and Hossein Aghababaei, *Senior Member, IEEE*

***Abstract*— Recently, the synthetic aperture radar tomography (TomoSAR) technique has attracted significant attention owing to its 3-D reconstruction capability of complex urban environments. The availability of a high number of images is usually a requirement for nonparametric spectral estimation methods. This letter evaluates the potential of four nonparametric spectral estimation algorithms, that is: 1) linear prediction (LP); 2) minimum norm (MN); 3) singular value decomposition (SVD); and 4) Capon for improved tomographic reconstruction of the third dimension of built-up areas with a small number of observations. The performance analysis is carried out for both simulated and real SAR datasets. The returns from the employed techniques indicate the efficient and low-computational estimator of LP by minimizing the average output signal power at the array of antenna elements and make it possible to separate multiple scatters at a distance below the Rayleigh resolution and clean sidelobes' phenomena in the elevation profiles. The experimental results of a dataset acquired by the TerraSAR-X sensor verify the effectiveness of the LP spectral estimator algorithm in the reconstruction of urban buildings. The estimated height of scatterers with the LP method is considerably similar to the ground-observed data.**

***Index Terms*— Building reconstruction, linear prediction (LP) method, nonparametric spectral estimation, synthetic aperture radar tomography (TomoSAR).**

## I. Introduction

IN RECENT years, due to different scatterers interfering from buildings, houses, roads, bridges, trees, and vegetation cover, the tomographic analysis of synthetic aperture radar (SAR) data in urban areas has become a valuable field of research. In the presence of steep topography, as vertical structures (i.e., buildings), severe signal contributions from multiple scatterers may superpose within in the same range-azimuth resolution cell [1]. To overcome this limitation, SAR tomography (TomoSAR) is a contemporary technique that has been attracting significant attention in the case of urban scenarios [2].

Manuscript received December 13, 2020; revised February 16, 2021 and April 5, 2021; accepted April 24, 2021. *(Corresponding author: Mahmod Reza Sahebi.)*

Mehrnoosh Omati and Mahmod Reza Sahebi are with the Faculty of Geomatics and Geodesy Engineering, K. N. Toosi University of Technology, Tehran 19967-15433, Iran (e-mail: momati@mail.kntu.ac.ir; sahebi@kntu.ac.ir).

Hossein Aghababaei is with the Faculty of Geo-Information Science and Earth Observation (ITC), University of Twente, 7514 AE Enschede, The Netherlands (e-mail: h.aghababaei@utwente.nl).

Color versions of one or more figures in this letter are available at https://doi.org/10.1109/LGRS.2021.3077517.

Digital Object Identifier 10.1109/LGRS.2021.3077517

3-D SAR focusing as an inverse problem can be solved using a variety of spectral estimation algorithms. Standard spectral estimators are categorized into three groups: sparsity-based compressive sensing (CS) approaches [3], parametric, and nonparametric methods [4]. CS-based TomoSAR techniques generally suffer from high computational consumption due to their iterative scheme and unavailability of adaptive algorithms for convex optimization [5]. Parametric algorithms assume a predefined statistical model that enables the estimation of the unknown model parameters. In these techniques, *a priori* knowledge is required about the number of interfering scatterers inside an azimuth-range pixel. Generally, parametric methods may represent significant estimates if the data happen to be close to the assumed model [6].

On the contrary, with nonparametric methods, there is no distributional assumption made regarding the nonparametric estimators; therefore, the number of parameters is estimated directly from the observed data [6]. Compared to the first two groups of methods, nonparametric estimators are fast and robust focusing techniques. These advantages make nonparametric spectral estimators more applicable to data processing. However, nonparametric techniques, such as beamforming and Capon, are typically limited by the relatively low potential in height resolution. Generally, the unavailability of a large number of image data with desirable baseline distribution impairs the resolution and quality of such reconstruction techniques.

In this letter, we investigate the problem of the requirement of the availability of a high number of images in nonparametric-based TomoSAR spectral estimation methods. The primary aim of this study is, thus, to improve the quality and accuracy of building height retrieval using a small number of TerraSAR-X stripmap data. We consider two new direction of arrival (DOA) estimation methods, namely, linear prediction (LP) and minimum norm (MN) for urban tomographic applications. The proposed nonparametric spectral estimation methods are evaluated with respect to their performance in the separation of the different scatterers at distances shorter than the Rayleigh resolution in urban areas. Interestingly, we prove that the LP method with constraints to minimize the average output signal power at the array of antenna elements offers the possibility to discriminate layover scatterers located below the Rayleigh elevation resolution and suppress the sidelobe effect.

This letter is organized as follows. Section II describes the theory of the two proposed DOA estimation algorithms. In Section III, the results on simulated data and stripmap

TerraSAR-X data are presented to highlight the potentials and limitations of the four nonparametric spectral analysis methods. Finally, the conclusion is provided in Section IV.

## II. Methodology

### A. Basic TomoSAR Theory

TomoSAR, as the extension of the 2-D SAR imaging principle, provides full 3-D imaging by forming a synthetic aperture along the orthogonal direction to the azimuth and the slant range directions. Due to the side-looking viewing geometry of SAR sensors, received echoes of the different scatterers with the same range of distance to the sensor may interfere within one resolution cell. In a stack of $N$ coregistered complex-valued SAR images, for a given pixel $(x, r)$ in the $n$th image, the integral of the backscattering function along elevation direction is represented by the following formula [7]:

$$g_n(x,r) = \int \gamma(x,r,s)\exp[-j2\pi\xi_n s]ds + \varepsilon_n(x,r)$$
$$g = A.\gamma + \varepsilon \tag{1}$$

where $\xi_n = 2b_{\perp n}/\lambda r$ is the spatial frequency along the elevation, $\lambda$ is the wavelength parameter, $r$ is the distance between the SAR sensor to the target, $b_{\perp n}$ is the perpendicular components of the spatial baseline for the $n$th sensor with respect to the master sensor, and the vector of $\gamma$ represents the complex vertical reflectivity of scatterers. Equation (1) illustrates the fundamental relationship between the multi-baseline signals and the complex-valued of the backscattered reflectivity profiles. Moreover, $\boldsymbol{\varepsilon}$ can be given as a Gaussian white noise vector.

By sampling $\gamma(s)$ in the elevation direction with $L$ steps, the steering matrix $\mathbf{A} = [\mathbf{a}_1, \mathbf{a}_2, \ldots, \mathbf{a}_L]$ with $N \times L$ dimension consists of $L$ steering vectors. The $N$-dimensional steering vector $a_l$ as a function of scatterer height can be given by

$$\mathbf{a}_l = \left[e^{(j2\pi\xi_1 s_l)}, e^{(j2\pi\xi_2 s_l)}, \ldots, e^{(j2\pi\xi_N s_l)}\right]^{\mathrm{T}} \quad (l = 1, 2, \ldots, L). \tag{2}$$

In (2), $s_l (l = 1, \ldots, L)$ is a discrete position along the elevation direction. The tomographic processing can be performed by different spectral estimation strategies to derive the reflectivity profile vector of, $\gamma$, each range-azimuth pixel. In Section II-B, we introduce two nonparametric approaches for this purpose.

### B. DOA-Based Estimation Methods in SAR Tomography

Data of the same target collected from multiple baseline SAR images can be considered as signals received by the individual array antenna [8]. Therefore, after the preprocessing of TomoSAR data (i.e., interferometric phase flattening and atmospheric phase compensation with PS-InSAR technique), different types of DOA estimation techniques can be applied for 3-D image focusing [3], [9]. This study compares and assesses two new nonparametric DOA algorithms for tomographic reconstruction of the built-up area to derive the accurate height of the buildings.

*1) Linear Prediction-Based DOA Estimation:* The LP estimation method, as a potentially valuable tool, is widely applied in the field of time series problems, speech processing, spectrum analysis, and array processing [10]. The basic concept of the proposed spectral algorithm is the minimization of the mean output signal power over the antenna array elements [11], [12]. Under this constraint, the SAR image target height can be reliably estimated in the noise presence.

Based on the idea of the LP estimator, using predictive coefficients, $\gamma(s_l)$, the value of $g_n$ is modeled by a weighted linear combination of $\exp[-j2\pi\xi_n s]$. Equation (1) in the LP estimator framework can be approximated as a discrete equation as follows:

$$g_n = \sum_{l=1}^{L} \gamma(s_l)\exp[-j2\pi\xi_n s_l] + \varepsilon_n$$
$$n = 1, 2, \ldots, N \; l = 1, 2, \ldots, L \tag{3}$$

where $\gamma(s_l)$ is the reflectivity power of elevation position $s_1$. The LP method, for each row of the steering matrix, finds the column vector of weights

$$\boldsymbol{\gamma}(s) = \left[\gamma(s_1), \gamma(s_2), \ldots, \gamma(s_L)\right] \tag{4}$$

which minimizes the quantity of the following criterion:

$$E\left\{|\boldsymbol{\gamma}(s)^H \mathbf{g}|^2\right\} = E\left\{|\boldsymbol{\gamma}(s)^H \mathbf{g}\mathbf{g}^H \boldsymbol{\gamma}(s)|^2\right\} = \boldsymbol{\gamma}(s)^H \mathbf{C}_{\mathbf{g}} \boldsymbol{\gamma}(s). \tag{5}$$

The constrained optimization problem minimizes the criterion subject to the constraint that the weight vector on the selected elevation position is unity. This constraint can be written using as [12]

$$\boldsymbol{\gamma}(s)^H \mathbf{u} = 1. \tag{6}$$

The column vector $\mathbf{u}$ is the $i$th column of an identity matrix $\mathbf{I}_{N\times N}$. In LP spectral estimator, as a multilooking method, the estimation of the covariance matrix is achieved through the averaging of adjacent pixel values in both azimuth and range directions

$$\mathbf{C}_{\mathbf{g}} = E\left\{\mathbf{g}\mathbf{g}^H\right\} \approx \mathbf{C}_g = \frac{1}{M}\sum_{m=1}^{M} \mathbf{g}\mathbf{g}^H \tag{7}$$

where $E[.]$ and $(.)^H$ denote the Expectation and Hermitian operators, respectively. The parameter of $M$ is the total number of neighboring pixels that need to be averaged. In this letter, to estimate the sample covariance matrix, we consider a $5 \times 5$ pixel window.

Using the method of Lagrange multipliers, the resulting optimal LP weight vector of the LP estimator can be solved as [11], [12]

$$\boldsymbol{\gamma}_{\mathrm{opt}}(s) = \frac{\mathbf{C}_g^{-1}\mathbf{u}}{\mathbf{u}^H \mathbf{C}_{\mathbf{g}^{-1}\mathbf{u}}}. \tag{8}$$

Corresponding to the autoregressive (AR) model for a signal, the estimated power spectrum of the LP method is computed by dividing the mean square prediction error and the magnitude squared spectrum of the prediction weights.

Thus, the power spectrum can be represented in the form of [11], [12]

$$\mathbf{P}_{\mathrm{LP}}(s) = \frac{\mathbf{u}^H \mathbf{C}_{\mathbf{g}}^{-1} u}{|\mathbf{u}^H \mathbf{C}_{\mathbf{g}}^{-1} \mathbf{A}|^2}. \tag{9}$$

The performance of the LP technique depends on the choice of column $\mathbf{u}$. To overcome this dependence, we adapted a criterion based on the maximum contrast of the reflectivity profile. In particular, the vector $\mathbf{u}$ is selected such that the reconstructed reflectivity profile has maximum contrast among the profiles that can be extracted from all possibilities of $\mathbf{u}$.

*2) Minimum Norm-Based DOA Estimation:* The MN is known as one of the typical high-resolution subspace-based DOA estimation techniques [13]. With this approach, after the estimation of the data covariance matrix $\mathbf{C_g}$, the widely used singular value decomposition (SVD) technique is performed to obtain the product of three decomposed matrices $\mathbf{U}$, $\mathbf{S}$, and $\mathbf{V}$ such that $\mathbf{C_g} = \mathbf{USV}^{\mathrm{T}}$. Then, the noise subspace eigenvectors are constructed by selecting the specific columns from $U$, i.e., $\mathbf{U}_{\mathrm{Noise}} = \mathbf{U}(:, q+1 : N)$. The parameter of $q$ corresponds to the $q$ largest eigenvalues.

In this method, the optimal solution for the weight vector $\mathbf{d} = [d_1, d_2, \ldots, d_N]^{\mathrm{T}}$ as a linear combination of noise eigenvectors is obtained by solving the optimization problem in the following way:

$$\min \mathbf{d}^H \mathbf{d}, \mathbf{U}_{\mathrm{Signal}}^H \mathbf{d} = 0, \quad \mathbf{d}^H \mathbf{e}_1 = 1 \tag{10}$$

where $\mathbf{e}_1$ is an $N \times 1$ vector with all elements equal to zeros, except for the first one (first column of the $N \times N$ identity matrix). The signal subspace matrix $\mathbf{U}_{\mathrm{Signal}} = [\mathbf{u}_1, \mathbf{u}_2, \ldots, \mathbf{u}_q]$ with $N \times q$ dimension is constituted by eigenvectors of the covariance matrix corresponding to the largest $q$ eigenvalues.

The spectrum function of this method is obtained based on the MN vector lying in the noise subspace, in which the first column of the identity matrix satisfies this condition. The optimization solution of (10) yields the MN spectrum estimator. This spectral estimator is performed from the following expression:

$$P_{\mathrm{MN}}(s) = \frac{1}{|\mathbf{A}^{\mathrm{T}} \mathbf{U}_{\mathrm{Noise}} \mathbf{U}_{\mathrm{Noise}}^H \mathbf{e}_1|^2}. \tag{11}$$

## III. Experiments And Results

In this section, the performance of employed spectral estimators is evaluated on simulated data and real TerraSAR-X images over Tehran, Iran. For the simulation of the tomographic SAR data based on the TerraSAR-X system parameters, we consider the problem of reconstruction of two scatterers within one resolution cell. The TerraSAR-X sensor parameters are shown in Table I, and the total baseline span is about 414 m and, thus, corresponds to the Rayleigh resolution of about 21 m in the vertical direction.

### A. Numerical Experiments

To explore the super-resolution capability of the estimators, in this simulated stack of SAR data, the layover scatterers are located at height differences lower than the Rayleigh resolution limit. Fig. 1 demonstrates the results of the reflectivity profile using four DOA estimation techniques on the simulated dataset. Moreover, to evaluate the capability of detecting double scatterers with the increased number of images, we have exploited three different values of the number of image acquisitions, $N = 19$, $N = 31$, and $N = 67$, although the total baseline is the same in all scenarios. This means that the simulated multibaseline datasets have identical Raleigh resolution in three cases. The results obtained in MN, SVD, and Capon estimators with simulated data reveal that, by increasing the number of acquisitions, the two scatterers whose elevation distance is smaller than Rayleigh resolution can be separately detected. The findings confirm that the nonparametric-based spectral estimation methods, such as MN, SVD, and Capon, require a high number of observations for reliable estimation and are strongly affected by the number of image acquisitions, while the analysis indicates that the proposed LP DOA estimation technique can correctly detect the location of two closely spaced scatterers as distinct scatterers with a reduced number of looks. This technique shows robustness to the number of images when the total baseline is kept constant.

TABLE I
TerraSAR-X Parameters

| Wavelength (m) | Range (km) | Incidence Angle | Slant Range Resolution (m) | Azimuth Resolution (m) |
|---|---|---|---|---|
| 0.031 | 563 | 25° | 1.2 | 3.3 |

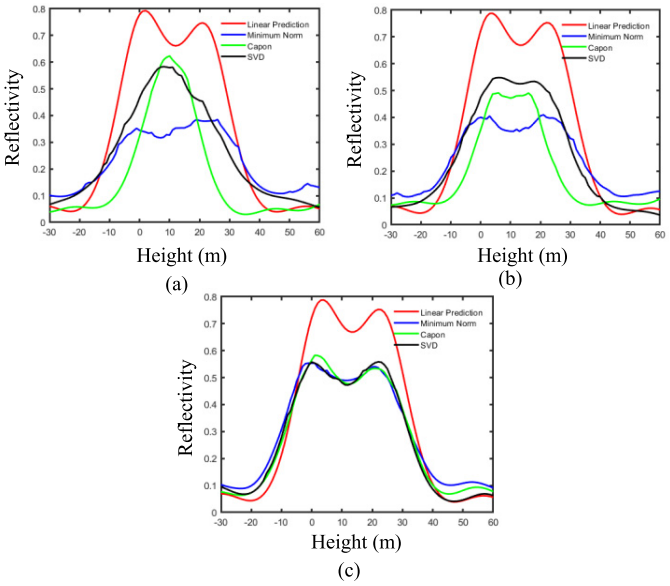


Fig. 1. Results of the reflectivity profile on the simulated dataset. (a) With 19 looks. (b) With 31 looks. (c) With 65 looks.

### B. Real Data Experiments

In this study, a stack of 19 stripmap images acquired by the spaceborne TerraSAR-X from descending orbits over the city of Tehran, Iran, was used. The data were obtained between 2012 and 2013, and the polarization mode of the images is HH. The study area belongs to a mosque located in

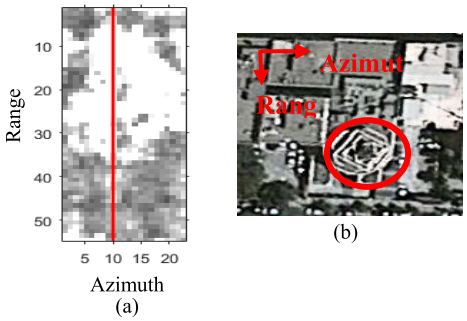


Fig. 2. Case study over a mosque. (a) Mean amplitude SAR image. (b) Location of a mosque on Google Earth.

Mirdamad Boulevard with a latitude of 35° 45' 34.19" N and a longitude of 51° 26' 15.54" E. The mosque and corresponding TerraSAR-X mean amplitude image are illustrated in Fig. 2. This test building, with an image size of 55 × 23 pixels, has a height close to 8.5 m, corresponding to an elevation range of 20 m. The mosque is a complicated study area with an elevation lower than the Rayleigh resolution.

In the implementation procedure of the proposed SAR tomographic methods for TerraSAR-X stripmap images, after the proper preprocessing of the stack datasets, two new tomographic imaging methods in the urban area now apply to evaluate the capability of detecting and separating multiple scatterers along the elevation direction.

The results of building height retrieval with the two DOA estimation methods are compared to the SVD and Capon spectral estimators. The validation of tomographic results is based on the ground truth of the height of the buildings.

*1) Results of Three TomoSAR Algorithms:* As can be seen, due to the effects of SAR imaging geometry in the target interaction, the location of the top of the mosque building is at the near range, while its bottom appears at the far range in the SAR image. In this study, the height differences below the Rayleigh resolution are estimated along the red azimuth line that occurs over the facade of the building of interest.

In this study, the quality of the proposed method can be expressed by the TomoSAR reconstruction with the reduction and suppression of sidelobes, super-resolution capability, and evaluation of the estimated tomographic heights with the ground-truth measurements. Fig. 3 shows the tomographic reconstruction of the considered line [see Fig. 2(a)] with the LP, MN, and Capon methods in the height-range plane.

At the intersection of the facade of the building with the ground surface, more than one scatterer mainly exists in the same image pixel. The experimental results indicate that the LP-based spectral estimation method considerably improves the TomoSAR imaging for the separation of layover contribution beyond the Rayleigh resolution limit. It can be seen at the beginning of Fig. 3(a) that the strong scatterer corresponds to the top of the building and the weaker scatterer caused by the reflection from the ground target. Fig. 3(e) illustrates the obtained reflectivity profile corresponding to the azimuth-range pixel at the beginning of the LP tomogram. As shown by the results of the LP spectral estimation method, with row pixels in the SAR image increasing, the difference

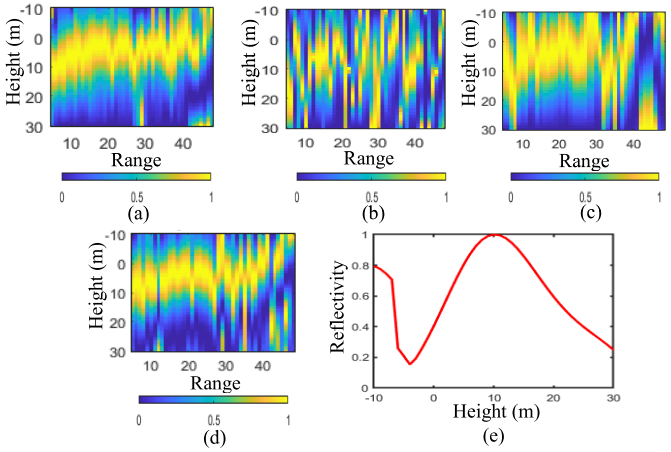


Fig. 3. Implementation of DOA estimation methods over a mosque area. (a) LP. (b) MN. (c) SVD. (d) Capon. (e) Reflectivity profile for the azimuth-range pixel at the beginning of the LP tomogram.

in elevation direction between the top and bottom portions of the building is 20 m. This estimation is considerably similar to the ground-truth data.

While the other employed TomoSAR methods, MN, SVD, and Capon, suffer from severe sidelobe issues, distinguishing between signal and noise components by SVD decomposition is a difficult task, especially when generating a tomogram that must handle different pixels, which may contain various numbers of scatterers, noise, and signal contributions. These three methods have not been able to resolve the layover and separate the overlaid scatterers located lower than the Rayleigh resolution. It is obvious that a height jump phenomenon can be seen in the tomograms obtained from the MN, SVD, and Capon estimator methods [see Figs. 3(b)–(d)]. The results affirm the fact that these techniques are highly affected by improper baseline distribution, while LP shows more robust reconstruction. Also, it is observed that there are significant differences between the estimated values along elevation direction and the real elevation range of 20 m. The estimated building values into the elevation direction extracted by using MN, SVD, and Capon TomoSAR techniques are 28, 15, and 18 m, respectively. As can be seen from Fig. 3(a), the estimated elevation range from the LP-based method is 20 m, which is consistent with the field-based measurement.

*2) Choose the Best Column for LP Estimator:* As it was mentioned before, choosing the column vector of the identity matrix has a significant effect on the results of the LP DOA method. In the present study, we propose a new method to choose the best column of the $N \times N$ identity matrix, by using the contrast criterion. Each pixel consists of $NL$-dimensional vertical reflectivity power vectors that resulted when different columns of the identity matrix are employed. For every pixel of the SAR image, this technique searches for vertical reflectivity power based on the maximization of the cost function. The following contrast cost function can be defined as

$$C\{\gamma(s)\} = \frac{\sqrt{\frac{1}{L}\sum_{m=1}^{L}\left(\gamma(s_m) - \frac{1}{L}\sum_{l=1}^{L}\gamma(s_l)\right)^2}}{\frac{1}{L}\sum_{m=1}^{L}\gamma(s_m)}. \quad (12)$$

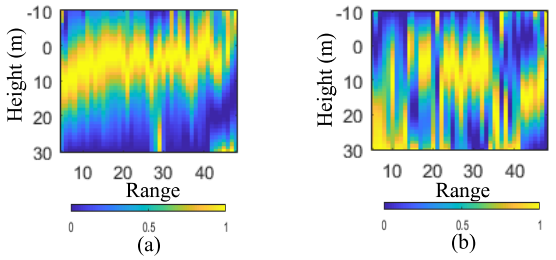


Fig. 4. Implementation of LP estimator. (a) Choosing the best column from the identity matrix. (b) Randomly select columns from the identity matrix.

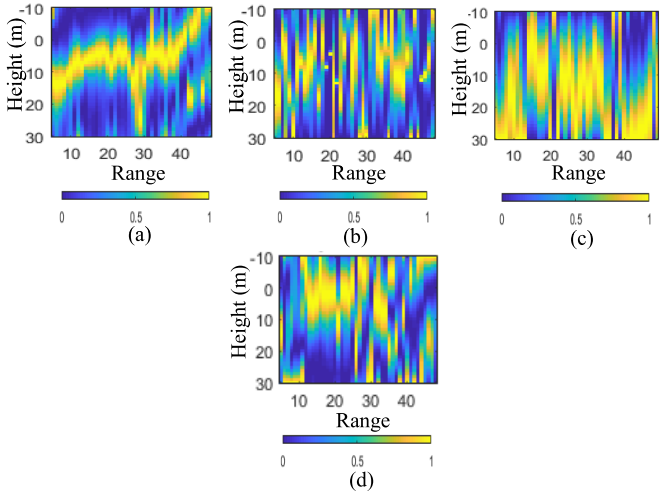


Fig. 5. Implementation of DOA estimation methods over a mosque area using ten SAR images. (a) LP. (b) MN. (c) SVD. (d) Capon.

The results of the proposed LP estimator using the best column and a random selection of the columns from the identity matrix are shown in Fig. 4(a) and (b), respectively. The outcomes indicate that the proposed optimal column selection approach enables the LP estimator to accurately reconstruct the height profile.

*3) Robustness of the DOA Estimation to the Number of Images:* In addition, we investigated and assessed the effectiveness of the employed nonparametric spectral estimators with respect to the reduced number of baselines in the focusing process. To this aim, half of the datasets (i.e., ten alternative acquisitions) are employed such that the overall baseline of ten images is the same as the one with all 19 images. In Fig. 5, the tomographic reconstruction results are illustrated for four different spectral estimators, LP, MN, SVD, and Capon. From the experiments, we can observe that the LP-based estimator algorithm retains TomoSAR reconstruction while reducing the required number of 2-D SAR images, indicating the robustness of this technique to the number of images. Instead, the SVD and conventional Capon methods are highly impaired by the reduced number of images, while the MN approach showed more robustness with respect to these techniques. Using a small number of SAR images, the height estimation results by LP, MN, SVD, and Capon methods are 23, 27, 40, and 24 m, respectively.

## IV. Conclusion

In this study, we evaluated two novel TomoSAR methods for improving the estimation accuracy of the height of the buildings in the urban environment. A stack of 19 TerraSAR-X stripmap images from descending orbits over the city of Tehran was processed. A building has been chosen as a case study, a low-rise mosque, to analyze the performance of the several nonparametric estimator methods. In this letter, among the employed DOA techniques, the LP nonparametric spectral estimation method enables layover contributions to be separated within each singular cell. Furthermore, the LP TomoSAR technique significantly improves the ability to suppress the sidelobes and reconstruct the reflectivity profile of the scatterers situated at a distance below the Rayleigh resolution. Estimates of heights using the LP TomoSAR method are consistent with the ground-truth values. Compared with other DOA estimation methods, such as MN, SVD, and Capon, the results show that the proposed LP estimator has a strong capability to reduce the impact of noise in the tomogram. The results also indicate the robustness of the LP estimator to the number of images.

## Acknowledgment

The authors would like to thank the Iran National Science Foundation (INSF) for generous financial support. They would also like to thank the European Space Agency (ESA) for providing the TerraSAR-X data images.

## References

[1] G. Fornaro, F. Lombardini, and F. Serafino, "Three-dimensional multipass SAR focusing: Experiments with long-term spaceborne data," *IEEE Trans. Geosci. Remote Sens.*, vol. 43, no. 4, pp. 702–714, Apr. 2005.

[2] A. Reigber and A. Moreira, "First demonstration of airborne SAR tomography using multibaseline L-band data," *IEEE Trans. Geosci. Remote Sens.*, vol. 38, no. 5, pp. 2142–2152, Sep. 2000.

[3] X. Zhu and R. Bamler, "Tomographic SAR inversion by $L1$-norm regularization—The compressive sensing approach," *IEEE Trans. Geosci. Remote Sens.*, vol. 48, no. 10, pp. 3839–3846, Oct. 2010.

[4] F. Gini, F. Lombardini, and M. Montanari, "Layover solution in multibaseline SAR interferometry," *IEEE Trans. Aerosp. Electron. Syst.*, vol. 38, no. 4, pp. 1344–1356, Oct. 2002.

[5] G. D. M. Del Campo, Y. V. Shkvarko, A. Reigber, and M. Nannini, "TomoSAR imaging for the study of forested areas: A virtual adaptive beamforming approach," *Remote Sens.*, vol. 10, no. 11, p. 1822, 2018.

[6] L. Wei, T. Balz, M. Liao, and L. Zhang, "TerraSAR-X StripMap data interpretation of complex urban scenarios with 3D SAR tomography," *J. Sensors*, vol. 2014, pp. 1–7, Jan. 2014.

[7] G. Fornaro, F. Serafino, and F. Soldovieri, "Three-dimensional focusing with multipass SAR data," *IEEE Trans. Geosci. Remote Sens.*, vol. 41, no. 3, pp. 507–517, Mar. 2003.

[8] T. Kato, H. Yamada, Y. Yamaguchi, R. Sato, S. Kojima, and M. Arii, "Fundamental study on multi-baseline SAR tomography using airborne X-band SAR," in *Proc. IEEE 5th Asia–Pacific Conf. Synth. Aperture Radar (APSAR)*, Singapore, Sep. 2015, pp. 15–19.

[9] G. Fornaro, F. Lombardini, A. Pauciullo, D. Reale, and F. Viviani, "Tomographic processing of interferometric SAR data: Developments, applications, and future research perspectives," *IEEE Signal Process. Mag.*, vol. 31, no. 4, pp. 41–50, Jul. 2014.

[10] J. Makhoul, "Linear prediction: A tutorial review," *Proc. IEEE*, vol. 63, no. 4, pp. 561–580, Apr. 1975.

[11] J. Gamba, *Radar Signal Processing for Autonomous Driving*, 1st ed. Tsukuba, Japan: Springer, 2020, pp. 62–86.

[12] D. H. Johnson, "The application of spectral estimation methods to bearing estimation problems," *Proc. IEEE*, vol. 70, no. 9, pp. 1018–1028, Sep. 1982.

[13] V. T. Ermolaev and A. B. Gershman, "Fast algorithm for minimum-norm direction-of-arrival estimation," *IEEE Trans. Signal Process.*, vol. 42, no. 9, pp. 2389–2394, Sep. 1994.